ORIGINAL PAPER

Unzipping flood vulnerability and functionality loss: tale of struggle for existence of riparian buildings

Dipendra Gautam[1,2,3] · Rabindra Adhikari[1,2,4] · Suraj Gautam[5] ·
Vishnu Prasad Pandey[2,4] · Bhesh Raj Thapa[2,6] · Suraj Lamichhane[2,4] ·
Rocky Talchabhadel[2,7] · Saraswati Thapa[4,8] · Sunil Niraula[9] · Komal Raj Aryal[10] ·
Pravin Lamsal[11] · Subash Bastola[4] · Sanjay Kumar Sah[4] · Shanti Kala Subedi[12] ·
Bijaya Puri[2] · Bidur Kandel[13] · Pratap Sapkota[14] · Rajesh Rupakhety[15]

Abstract

Floods pose significant risk to riparian buildings as evidenced during many historical events. Although structural resilience to tsunami flooding is well studied in the literature, high-velocity and debris-laden floods in steep terrains are not considered adequately so far. Historical floods in steep terrains necessitate the need for flood vulnerability analysis of buildings. To this end, we report vulnerability of riparian-reinforced concrete buildings using forensic damage interpretations and empirical/analytical vulnerability analyses. Furthermore, we propose the concept and implications of functionality loss due to flooding in residential reinforced concrete (RC) buildings using empirical data. Fragility functions using inundation depth and momentum flux are presented for RC buildings considering a recent flooding event in Nepal. The results show that flow velocity and sediment load, rather than hydrostatic load, govern the damages in riparian RC buildings. However, at larger inundation depth, hydrostatic force alone may collapse some of the RC buildings.

Keywords Flood risk · Flood vulnerability · Functionality loss · Flood performance · Fragility function · Riparian building · RC

1 Introduction

The changing climate narrative has risen the frequency and impact scenarios not only in environmental variables but also in the built environment, portraying aggravation in terms of damage and losses. Floods are known to be more devastating over the years due to their multi-faceted and ever-widening dimensions, especially in terms of structures and infrastructure damage. Recent flood events such as the 2017 central Nepal, (Thapa et al. 2020; Gautam and Dong 2018; Adhikari et al. 2019), 2019 flood in Italy and Austria (Fuchs et al. 2019a, b), 2015 flood in Italy (Santo et al. 2016), 2011 flood

✉ Dipendra Gautam
  dipendra01@tcioe.edu.np

Extended author information available on the last page of the article

in Korea (Kang and Kim 2016), 2005 flood in Romania (Godfrey et al. 2015), and many other events have highlighted the severity of damage and losses and in the built environment. Flood vulnerability analysis of residential buildings is gaining attention over the past decades using both analytical and empirical approaches. Fuchs et al. (2019a, b) presented a comprehensive account of flood vulnerability analysis methods. Analytical and hybrid (analytical and empirical combined) flood vulnerability studies are relatively rare in comparison to the empirical ones. Flood vulnerability of structures and infrastructures is commonly presented in terms of depth-damage curves using empirical damage data (see e. g., Gautam and Dong 2018; Thapa et al. 2020; Fuchs et al. 2019a, b; Fuchs et al. 2019a, b; de Risi et al. 2020; Baradaranshoraka et al. 2019). The key issues regarding flood vulnerability analysis are the underlying epistemic and aleatoric uncertainties. Factors such as inundation depth, flood exposure time, sediment extent in flowing water, buoyancy effects, debris damming mechanism, etc., are associated with uncertainties and natural variability, which make analytical vulnerability modeling a challenging task. Experimental studies can alleviate these challenges to some extent, but they are often associated with unrealistic costs. In the published literature, tsunami and debris flow vulnerability analyses are more commonly reported than flood vulnerability analyses. Tsunami vulnerability/fragility of residential buildings using empirical and analytical models are reported by several researchers (Karafagka et al. 2018; Park et al. 2017; Reese et al. 2011; Petrone et al. 2017; Suppasri et al. 2012; Koshimura et al. 2009). Similarly, debris flow analysis is considered in vulnerability analysis of structures and infrastructures (Jakob, Stein, and Ulmi 2012; Prieto et al. 2018; Kang and Kim 2016; Ciurean et al. 2017). On the other hand, few studies have incorporated flood damage and loss analyses (Komolafe, Herath, and Avtar 2019; Ciurean et al. 2017; Valencia et al. 2011; Amadio et al. 2019). Flood vulnerability analysis together with functionality loss and economic loss is very crucial to be determined since the occupants are naturally anxious regarding the re-occupation of their houses. In seismic regions, construction of reinforced concrete structures is generally guided by either seismic codes or some form of regulations, which is instrumental when it comes to flood performance of buildings and other structures since structures with earthquake resistant provisions have some degree of resilience against flood-induced horizontal forces. Impulsive loads induced by flowing water and debris impact loads can challenge even the code compliant reinforced concrete structures. Lesser structures such as unreinforced masonry and other brittle construction forms cannot be expected to safely withstand a major high-velocity flood and the debris load it carried. Even in structures with adequate resistance to lateral loads, secondary effects such as toe cutting, and erosion of foundation and other components lead to drastic failure mechanisms. To this end, understanding vulnerability of reinforced concrete riparian buildings is important and of great interest.

Apart from physical damage to the structures, indirect impacts such as loss of functionality and economic values need to be considered in evaluating flood resilience of riparian communities. Functionality loss due to flood damage in buildings is not adequately addressed in the literature, and there is a need to develop a framework for this important aspect of resilient riparian communities. To address these gaps in the literature, we use empirical data obtained from field reconnaissance conducted by experienced surveyors after the 2021 Melamchi River flood in central Nepal. Damage to buildings and other infrastructure are described with various examples and observations from the field. Flood vulnerability function and functionality loss function are created using the field data. We also present empirical flood fragility functions for reinforced concrete buildings damaged by the Melamchi River flood.

2 Setting the scene: the 2021 melamchi river flood in central Nepal

On June 15, 2021, a devastating flood event occurred in the Melamchi River of Indrawati River Basin in central Nepal. The flood displaced 525 families, resulted in 337 household damage, killed five and injured six people, and left 20 people unaccounted for (Pandey et al. 2021). The flood damaged 13 foot trail bridges, seven reinforced concrete (RC) bridges, a hydropower project, and the headwork of the Melamchi Water Supply Project leading to enormous economic loss, which is not collectively estimated yet. All the damage and losses incurred due to this event were confined within Sindhupalchowk district, which is also the most affected district by the 2015 Gorkha earthquake in Nepal. Ground shaking due to the earthquake initiated massive slope instabilities and mass movement in the region. The unstable slopes were subsequently subject to torrential precipitations every summer in the following years. Due to such exposure, landslides and mass movements were triggered in 2021, leading to debris-laden floods. The Melamchi River flood mainly affected Melamchi and Chanaute settlements. An example of damage in Melamchi neighborhood is shown in Fig. 1a. Figure 1a highlights that many buildings were constructed in a debris fan and riverbank and thus were either washed away or heavily sedimented or damaged. Due to riverbed aggradation and subsequent channel migration, almost all buildings situated on

Fig. 1 **a** Damage scenario after the Melamchi River flood in: **a** Melamchi neighborhood, **b** Chanaute neighborhood

the riverbank were affected by the flood. It is interesting to note that RC building resisted flood entry significantly, so the impact had deterred in the areas that did not face the riverbank directly. Due to the gentle riverbed slope, we did not observe any boulder impact on buildings in Melamchi neighborhood. On the contrary, Chanaute neighborhood observed the scenario in which large boulders directly impacted the buildings, leading to significant damage to collapse as shown in Fig. 3b. Notably, the riverbed slope in Chanaute neighborhood was considerably steep, so the flood event transported heavy boulders.

2.1 Flood performance of buildings

Hydrostatic, hydrodynamic, impulsive, debris impact, and debris damming are the common forces that are imposed against the face of the buildings exposed to flood (Federal Emergency Management Authority 2017). The water profile-based hydrostatic action occurs when inundation takes place. Hydrodynamic force is often the most challenging action experience by buildings subjected to high-velocity floods. Hydrodynamic action is largely governed by the velocity of flow, impulsive action, and extent and size of debris. In the case of steep riverine floods, combined action of flood and mass movement results in debris-laden flow, as was the case of the 2021 Melamchi flood in central Nepal. Most of the upstream slopes were stirred by the 2015 Gorkha earthquake and led to landslide dam outburst flooding transporting an enormous volume of debris. Testimonies of debris transportation for more than 25 km stretch was observed during the field reconnaissance. Figure 2 shows the effects of debris-laden flooding in residential buildings in Melamchi neighborhood. As seen in Fig. 2, when the terrain slope gets milder, the velocity of flow decreases, and sediment flow controls the flood regime depositing sediments in buildings through openings. Due to considerably low velocity and the absence of large sediments

Fig. 2 Manifestations of debris-laden flooding in Melamchi (27.830680 N, 85.575513E): **a** debris (fine sand) deposition up to the first story in an engineered RC building, **b** debris (fine sand) deposition in an under construction RC building, **c** RC building filled with debris due channel shifting due to the flood, **d** partly submerged under construction RC building, **e** completely submerged single storied RC building with exposed reinforcements left for story extension, **f** about to collapse RC building due to foundation erosion

(boulders), structural and nonstructural components of RC buildings are barely damaged. Figure 2f shows a near collapse code non-compliant RC building due to foundation erosion. Due to channel shifting, the Melamchi flood caused substantial damage to many buildings that were assumed to be above the flood level. Debris-laden flooding and subsequent debris deposition in the main river channel were responsible for damage to buildings and structures above the flood level.

Figure 3 shows flood damage to RC buildings in Chanaute neighborhood, approximately 25 km upstream of the Melamchi neighborhood. Large boulders were also observed along the riverbank that struck many riparian RC buildings which suffered greater devastation than that those in Melamchi. In this neighborhood, several buildings suffered collapse of structural members such as columns, beams, and floor slabs. Many such collapses were due to boulder impact. Meanwhile, damage to nonstructural components such as infill walls was mainly due to debris-laden flooding which generates lateral pressure against the walls. Even examples of damage due to impact of tree trunks and cobbles carried by the flood were observed (see Fig. 3). Nonstructural components such as shutters used for partitioning were affected even when not exposed to cobbles or tree trunks.

Some spectacular observations were made during the field reconnaissance regarding flood performance of RC buildings as shown in Fig. 4. When exposed to storm surge or inundation with clear water, ground or the first story of a building are often most damaged. When the flood carries massive debris, impact loads can damage building components at higher levels as shown by the damaged column in the second story of a building shown in Fig. 4. Unlike seismic loading, debris impact load is not proportionally distributed with building mass but is rather concentrated near impact points. Local stress concentrations generated by such impacts can have devastating effects on building components. RC buildings, by virtue of their resistance to flow-induced loads, divert flood current. The diverted current imposes high intensity loads near the corners of the buildings. These phenomena of local impact and flow diversion result in damage

Fig. 3 Manifestations of debris-laden flooding in Chanaute (27.902162 N, 85.543736E): **a** damage to shutters used for partitioning, **b** close-up view of flood damage to the ground story that shows debris deposition, **c** collapsed and heavily damaged shutters, **d** collapsed columns and slab due to boulder impact, **e** damage to structural and nonstructural components due to debris impact
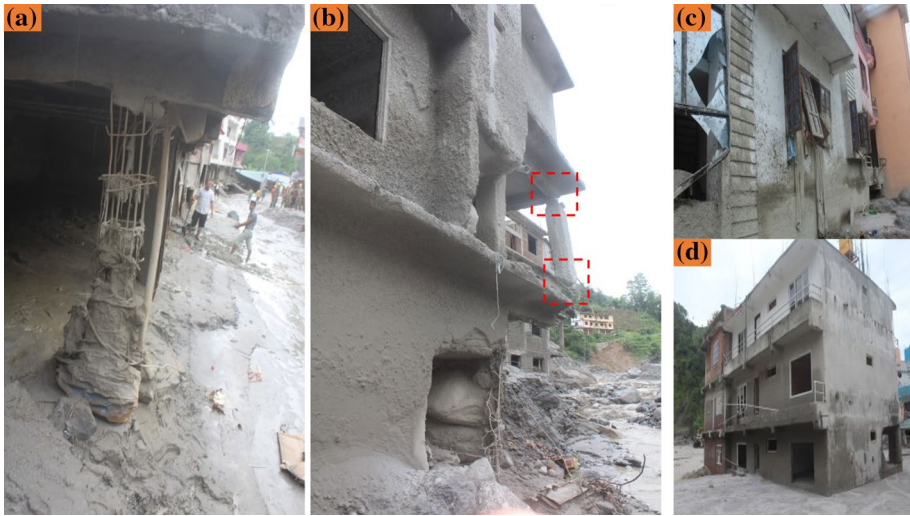
Fig. 4 Damage to RC buildings due to flood: **a** collapsed brick infill walls, **b** heavily damaged walls and column damage, **c** partially collapsed faces of ground and first stories and heavily damaged corner column of the second story, **d** collapsed brick infill walls, **e** column damage due to debris impact

concentrations and localized failures, which can subsequently lead to global failure of the buildings. Apart from this, waterways formed by debris impact leads to erosion of building components as well as severe damage to areas around the waterways where the flow velocity is high.

In substandard RC construction, debris-laden floods can easily erode concrete and leave just the reinforcements behind as shown in Fig. 5. This can lead to local failure, and in the lack of structural redundancy, continued flooding can aggravate damage leading to potential collapse. Structures exposed to prolonged debris-laden floods are thus prone to progressive collapse. Flood water intrusion can also dislocate window frames and damage windows because window frames are generally not adequately anchored to structural components or infill walls.

In Melamchi, flood caused substantial damage even to engineered RC buildings. As shown in Fig. 6a, an RC building with seismic bands intended to protect against out-of-plane collapse, failed. Lack of anchorage of the band and the wall to the main structural system leads to such vulnerabilities. Moreover, infill walls, which have the maximum thickness of 230 mm in the buildings studied here, do not seem to have adequate resistance to debris-laden flooding. Figure 6 shows examples of damage to RC buildings and components when fine sediments are more prominent than large boulders. Metal shutter gates in the lower floors were often found to be damaged, leading to aggravation in overall damage of the buildings.

Foundation erosion and subsequent damages were observed in non-RC residential buildings as shown in Fig. 7. Plinth beams in RC buildings seemed to hold the columns effectively together. In masonry buildings, the lack of integral connection between orthogonal walls led to severe damages. Steel structures without proper anchorage to the foundation were also severely damaged. Toe cutting was responsible for damaging many stone masonry and substandard RC buildings. Debris impact destroyed many tubular steel-frame buildings as shown in Fig. 7.

Fig. 5 Damage to RC buildings due to flooding: **a** eroded column depicts remains of reinforcements of a substandard RC building, **b** progressive damage to an RC building due to debris-laden flood, **c** damage to window frames due to flood entry inside an RC building, **d** damaged infill walls and sediment deposition in two stories of an RC building
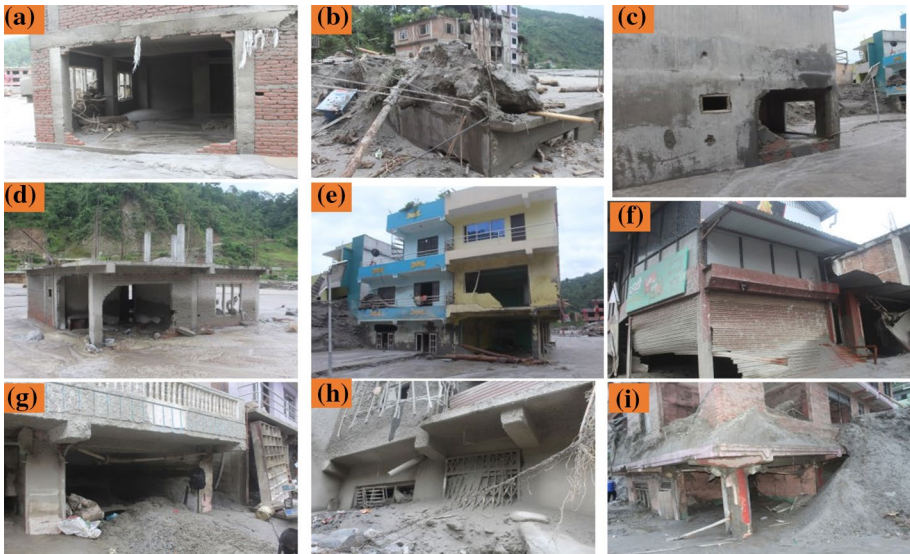
Fig. 6 Damage to RC buildings due to flooding: **a** out of plane collapse of infill wall of an engineered RC building, **b** damage to RC column and distortion of longitudinal reinforcements, **c**, **d**, **e** infill damage at the corner locations, **f** damage to shutter used for shop outlets, **g** damage to shutter frame, **h** damage to steel grills provided in openings, **i** infill walls collapse in first and second stories due to debris attack

Fig. 7 Flood damage to buildings: **a** foundation damage and damage to block infill masonry, **b** damage to infill panels, **c** damage to RC foundation, **d** foundation erosion in an RC building due to toe cutting, **e** foundation damage in a steel building due to toe cutting, **f** distortion in tubular steel post due to debris impact

# 3 Conceptualization and formulation of flood vulnerability and functionality loss

3.1 Empirical approach

3.1.1 Vulnerability analysis

The inundation depth was measured in situ using measuring tape from plinth to the flood mark level. In some cases, the depth was estimated by counting the number of stories. The damage extent was assigned in a percentage value that adheres to the fraction of total replacement cost. Damage ratio was assigned based on expert surveyors' evaluations. The damage to structural components, such as columns and foundations, leads to greater damage ratio. On the other hand, damage to nonstructural components, such as infill walls and parapet walls, leads to lower damage ratio. We collected damage ratio and inundation depth for 69 RC buildings along the Melamchi and Chanaute stretch of the Melamchi River. We used inundation depth as the intensity measure (IM) to create empirical vulnerability function as shown in Fig. 8. Based on the coefficient of determination, after trialing several functional forms, we found the logistic function as the most representative. Other researchers have also used logit function to model empirical data to create loss and damage functions (e. g. Bessason et al. 2022). The functional form of logistic function can be presented as:

$$\text{logit}(p) = \log\left(\frac{p}{1-p}\right) \tag{1}$$

where p is the probability and $\frac{p}{1-p}$ is odds that correspond the probability.
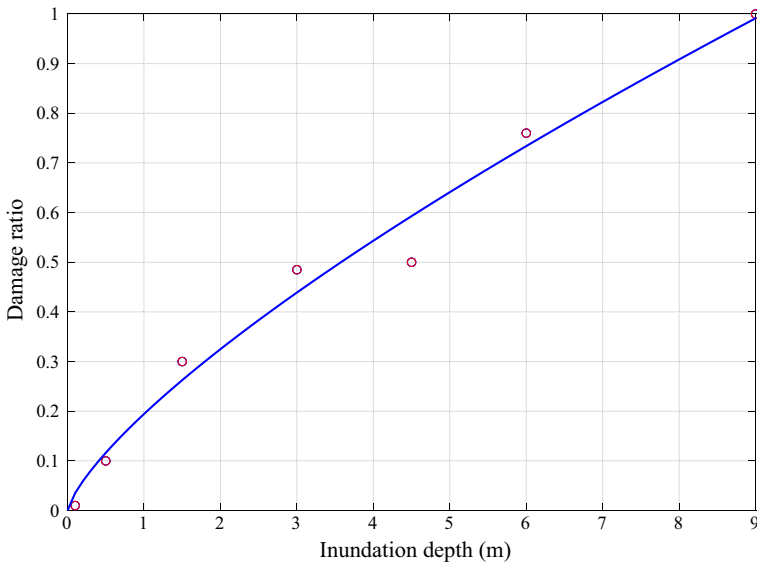
Fig. 8 Empirical flood vulnerability curve for RC buildings

For multiple buildings with the same IM value, we averaged the damage ratio and fitted the vulnerability function. For up to 3 m inundation, the damage ratio is less than 50% and it reaches 75% if 6 m inundation (roughly correspond to two stories) takes place.

Vulnerability functions indicate the mean damage ratio of a particular structure/infrastructure under a particular IM value. Vulnerability can be more representatively presented in terms of fragility functions which indicate the probability of reaching or exceeding a particular damage/performance level under the given value of the IM. We adopt three damage classes to disaggregate the total data as minor to moderate, major to severe, and extensive to collapse. The minor to moderate damage state indicates the damage ratio up to 25%, major to severe corresponds to damage ratio between 25 and 70%, and extensive to collapse corresponds to greater than 70% damage ratio. Among the 69 case study buildings, 16 buildings were categorized under minor to moderate damage state, 35 buildings were categorized under major to severe damage state, and 18 buildings were categorized under extensive to collapse damage state. Since we have limited data, we are not able to define more distinct classes, and thus three broad damage states are defined to create fragility functions. For any damage state (D), the likelihood (L) of the fragility function (F_D) can be represented as in Eq. (1):

$$L = \prod_{i=1}^{N} \left[F(D_i)\right]^{x_i} \left[1 - F(D_i)\right]^{1-x_i} \tag{2}$$

where $F(D)$ indicates the fragility function for the damage state D that indicates minor to moderate and so on, a_i represents the IM value corresponding to the building I, x_i is 1 or 0 based on whether the damage state is exceeded at building i, and N corresponds to the total number of buildings. The lognormal fragility function is dominantly used for empirical data to construct fragility functions as suggested by many researchers worldwide (e. g. (Shinozuka et al. 2002; Porter, Kennedy, and Bachman 2007; Gautam 2018; del

Gaudio et al. 2019; Gautam et al. 2018; Gautam et al. 2021; Gautam et al. 2019; Gautam and Rupakhety 2021; Gautam et al. 2020) A two-parameter lognormal cumulative fragility function, F(D), can be represented as:

$$F(D) = \Phi \left[\frac{1}{\beta} \ln \left(\frac{a}{\alpha} \right) \right]$$ (3)

where $\Phi[\cdot]$ is standard normal distribution function and α and β are the lognormal fragility function parameters, viz. median and lognormal standard deviation, respectively. The values of α and β are estimated by maximizing the likelihood function as follows:

$$\frac{d \ln (L)}{d\alpha} = \frac{d \ln (L)}{d\beta} = 0.$$ (4)

Using the maximum likelihood estimate, we estimated lognormal fragility function parameters, as summarized in Table 1.

Using the parameters of Table 1, flood fragility functions for RC buildings are constructed as shown in Fig. 9. Figure 9 shows that due to limited data for minor to moderate damage state, their fragility functions tend to converge to the major to severe damage state after 10 m inundation depth. The fragility function for extensive to collapse damage state highlights a 50% exceedance probability at ~7 m inundation depth. Extreme events such as the 2021 Melamchi River floods are expected to result in inundation depth even greater than 7 m, and thus the likelihood of observing extensive to collapse damage state in most of the RC buildings is very high. Meanwhile, most of the shallow inundation (< 1.5 m) is found to be insignificant for RC buildings, unlike the wattle and daub constructions as reported by Thapa et al. (2020).

3.1.2 Functionality loss analysis

Structures and infrastructures are constructed with a purpose. Flood events can either damage the structure or sometimes leave the structures filled with debris. In the latter case, significant damage would not occur in any member, but there exists a period between flood event and re-occupation of the building. In most cases, buildings that sustained slight to minor damage are also used with minor repairs or even without repair as insurance and subsidies are sanctioned after a considerable time only. In this context, based on the field survey that we conducted on 72 RC buildings after the Melamchi flood, including the majority of RC buildings that sustained minor to moderate damage, we postulate a concept of functionality loss. Functionality loss signifies the loss of operation of a particular structure/infrastructure for a defined period of time. It is

Table 1 Lognormal fragility function parameters for RC buildings

Damage state (D)	Lognormal fragility parameter	
	Median inundation depth [m] (α)	Lognormal standard deviation (β)
Minor to moderate	3.52	0.71
Major to severe	4.55	0.59
Extensive to collapse	6.80	0.35
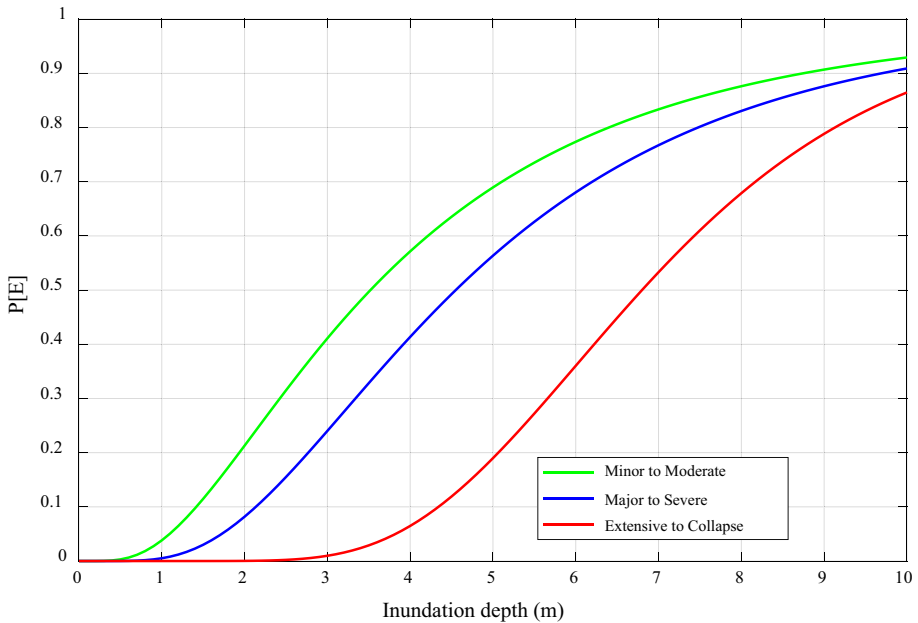
Fig. 9 Empirical flood fragility functions for RC buildings

expected that functionality loss decreases with time as repair and retrofitting is carried out. As a quantitative measure of loss, we use the ratio of out-of-use to total plinth area as a measure of functionality loss. Functionality loss is best modeled as an evolving process (see e. g., Rupakhety and Sigbjörnsson 2014) which requires a series of functionality evaluation after a damaging event. Since we only have one survey, which was a week after the flood, our functionality loss model is only a snapshot in time of an evolving process. Functionality loss percentage for each of the 72 buildings surveyed during the field assessment was assigned based on the status of building use as per plinth area. For example, if the ground story has debris deposition and is not cleared until the designated period, then the ground story cannot be used for any purpose, be it storage, a shop outlet, or even residential space. While assigning the functionality loss ratio, we also noted the inundation depth. Functionality losses in buildings with similar inundation depths were averaged. The averaged losses are then fitted to a logistic model as shown in Fig. 10. It should be noted that 100% functionality loss occurs if the inundation depth is more than 4 m, which corresponds to one and a half stories inundation. This is expected because of several reasons. First, access to higher stories is disrupted when the lower stories are filled with debris. In addition, psychological concerns about impending damage leads to disrupted use of the unaffected floors. Functionality loss functions such as these can be used for planning temporary shelters in the case of similar flood events. It is expected that functionality losses in less resilient constructions such as unreinforced masonry is higher.
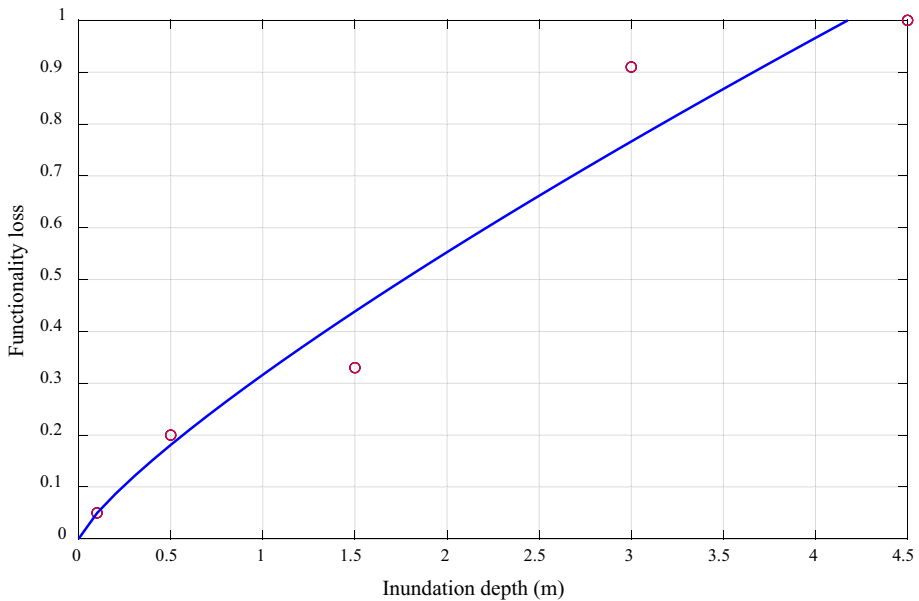
Fig. 10 Functionality loss function for RC buildings

3.2 Analytical approach

3.2.1 Case study building

Most of the buildings constructed before 2012 in Nepal do not comply with the earth-quake resistant guidelines that were suggested in the form of mandatory rules of thumb (MRT). Before 2012, structural drawings and detailing were not required to get building permit, hence almost all RC buildings were constructed without proper structural details using local knowledge and state of the art practice. Also, several buildings constructed even after 2012 in most parts of the country do not comply since only a few municipalities have mandated structural designs and details so far. If not compliant, such buildings are often constructed with a rule-of-thumb practice using 9″9″ (230,230 mm) column, 9″13″ (230,330 mm) beam, 4″ (100 mm) slab, and 4′4′ (1.2·1.2 m) footing pad. We considered a case study building of the same structural dimensions and configuration. A representative floor plan of the case study building is shown in Fig. 11. The building is a rectangular five-storied RC building. The beam and column section details are presented in Figs. 12 and 13, respectively. The building configuration, geometrical details, and parameters used for finite element modeling are summarized in Table 2.

3.2.2 Finite element analysis

Despite the dead and live loads, buildings are subject to a combination of several loads during a flooding event. The Federal Emergency Management Authority (FEMA) states that a building under tsunami impact will be subject to hydrostatic, buoyant, hydrodynamic, impulsive,
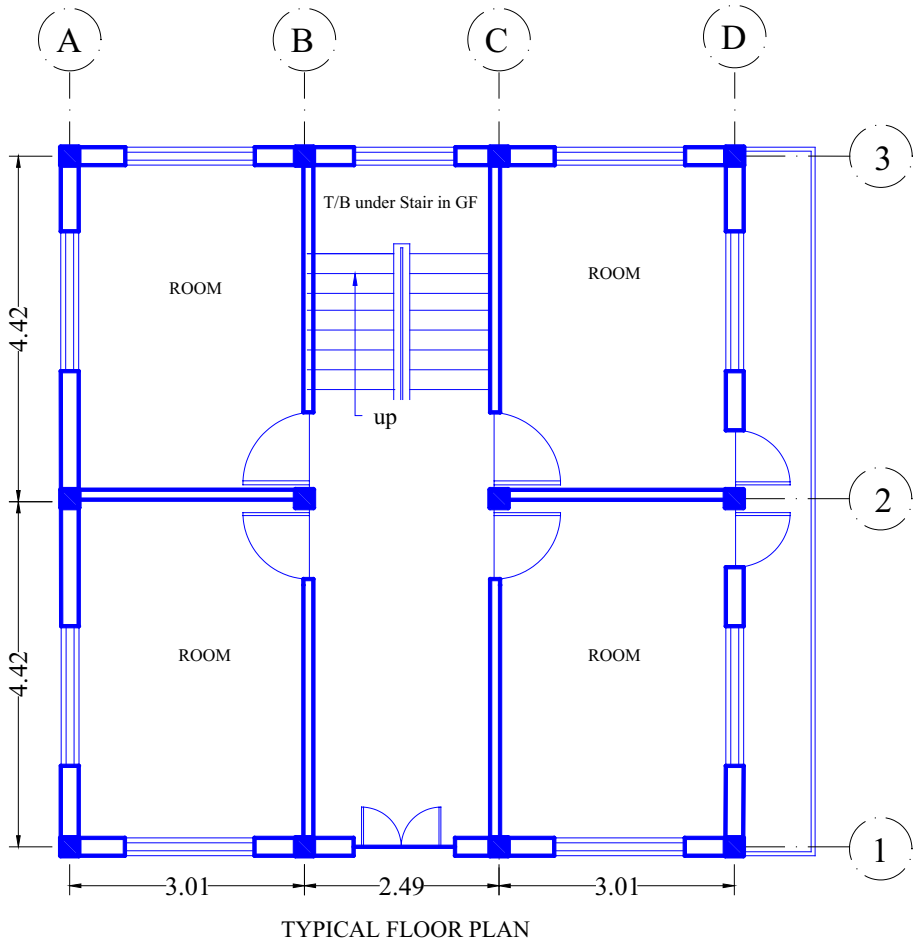
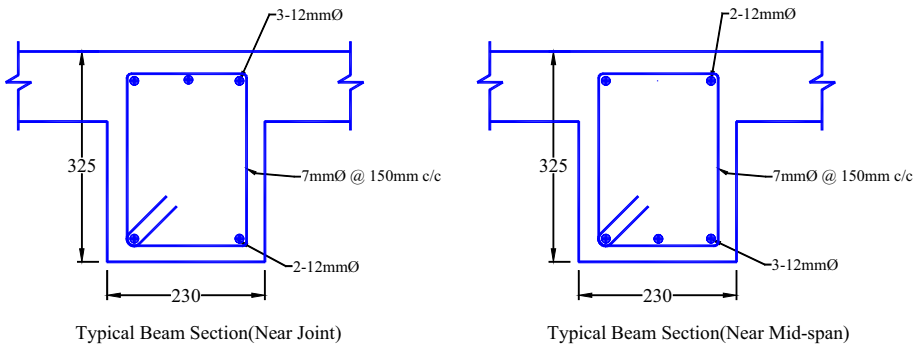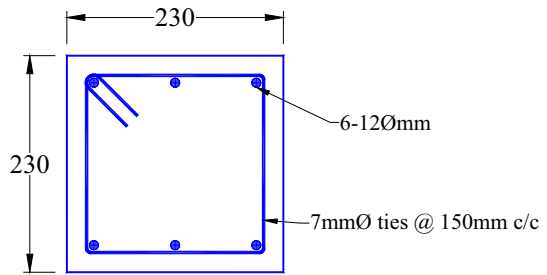**Fig. 11** Typical plan of a residential RC building in Nepal used as a case study

Fig. 12 Typical sectional details of beam at joint and mid-span

Fig. 13 Typical column details of the case study building

Table 2 Geometric and material properties used for finite element modeling

| Component	Description	Data
Frame	Type	Moment resisting frame (MRF)
	No. of stories	5
	No. of bays in X-direction	3
	No. of bays in Y-direction	2
	Story height	2.87 m
	Total width along X-direction	8.74 m
	Total width along Y-direction	9.07 m
	Size of beam	230 325 mm
	Size of column	230 230 mm
	Thickness of slab	100 mm
Load	Live load at floor slab	2.5 KN/m²
	Live load at roof	1.5 KN/m²
	Staircase load	3 KN/m²
	External wall load	8.98–12.83 KN/m
	Internal wall load	4.86–6.94 KN/m
	Isolated square footing	1.2 1.2 m, 1.5 m below plinth
Material	Grade of concrete	20 MPa for all concrete members
	Grade of steel rebar	Fe-500 for all RCC members
	Brickwork	7.5 MPa bricks in 1:6 cement-sand mortar for 230 mm thick walls

debris impact, and debris damming forces (Federal Emergency Management Authority 2017). The hydrostatic force is developed due to the force exerted by the standing water against the structural components. The buoyant force is also a type of hydrostatic force which arises due to submergence of structure and subsequent water displacement. For the moderate to high-velocity flows, hydrodynamic forces become significant. The hydrodynamic forces imposed on the face of structure can be estimated using the approach suggested by FEMA (Federal Emergency Management Authority 2017) as follows:

$$F_{\text{hyd}} = K_d \left[0.5 \rho_s C_d B \left(h v_f^2 \right) \right] \tag{5}$$

where F_{hyd} indicates hydrodynamic force, K_d is the modifier that accounts for both low and high forces due to mechanisms such as shielding and has gotten its nominal value 1, ρ_s is

the fluid density, C_d is the drag coefficient with a value of 2 which is defined by FEMA P-646, and hv_f^2 indicates the median value of maximum momentum flux. Despite hydrostatic and hydrodynamic forces, we also considered impulsive action as a considerable force is expected by the impact of the edge of the surge of the water on the exposed face of the building. The impulsive action increases the hydrodynamic action; thus, we used 1.5 as a multiplier to the hydrodynamic force estimated as per Eq. (5) (Federal Emergency Management Authority 2017). Since we do not have confirming evidence of debris impact and debris damming, quantification of both of these parameters was not possible. Accumulating the dead, live, hydrostatic, and modified hydrodynamic forces, we created a finite element model of the case study building in SAP 2000 *v*.23 (Computers and Structures Inc. 2013). A 3D finite element model of the case study building is shown in Fig. 14.

The beams and columns are modeled using 1D (line) elements with appropriate sections including reinforcements. The stiffness of the slab is neglected in the analysis, and loads from slabs are distributed to beams using the 'none' slab section. The building is modeled up to the foundation top level, which is 1.5 m below the plinth level and includes a plinth beam as well. Nonlinear hinges were assigned at each end of beam and column elements at a 10% distance of member length from the joint. Nonlinearity of frame is captured only at frame-hinge locations. The change in stiffness in the building due to infill walls is not considered in this model. As the loading in the structure is due to floods acting on some parts of the building only, the capacity curve for the building was obtained by performing pushover analysis in which static nonlinear analysis was carried out under displacement-controlled incremental loading, matching the flood load including the P-Δ effects. The deformation is significant within the inundation height only, the central joint in the story nearest to the flood level was considered to obtain the capacity curve which was done for incremental flood-velocity by preloading with the dead load, 30% of the live load, and total hydrostatic load. From the pushover analysis, we obtained yield and ultimate forces. Based
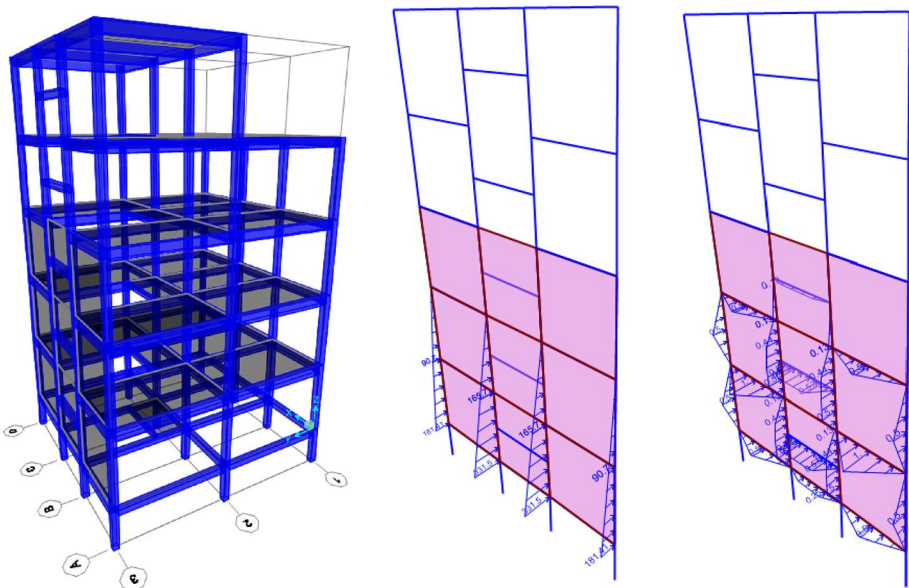
Fig. 14 Finite element model of the case study building

on the yield and ultimate force values, three damage states were defined as suggested by the HAZUS Tsunami Model Technical Guidance (Federal Emergency Management Authority 2017). The moderate damage corresponds to the yield force, extensive damage corresponds to the average force of yield and ultimate forces, and the complete damage corresponds to the ultimate capacity of the structure. Using the same approach suggested for tsunami force, we estimated capacities of three damage states. Thereafter, we analyzed the building considering dead load, live load, hydrostatic load, and modified hydrodynamic load for 0.375, 0.75, 1.125, 1.5, and 1.875 m/s scenario velocities. Similarly, we considered inundation depths up to 2.87 m to replicate various inundation scenarios. The velocity range was selected in such a way that the last analysis was performed just below the ultimate load limit since higher velocities were found to result in sudden collapse of the structure. Based on the finite element modeling, it is observed that the empirically estimated velocities are too high to be sustained by the existing buildings. This means the inundation depth is rather deterministic, the empirically determined velocity, if implemented in finite element models, sudden collapse occurs and none of the existing buildings are expected to survive. Thus, uncertainties are rather constrained within velocity estimation. In this context, we adopted a range of velocities to obtain a range of demand values for statistical fitting. To reflect the variation on inundation depth as observed in the field, we considered first and second story inundations, which correspond to 2.87 m and 5.74 m depths. Although the third-story inundation was observed in a few buildings, our analysis resulted in the collapse of the structure due to dead load when two-story inundation was considered. Thus, the damage incurred by the two-story and three-story inundations should be more aligned to static loading, or some of the collapsed and swept away buildings should have reflected the sudden collapse scenario too.

Although empirical fragility models reflect the realistic scenarios of inundation, velocity, debris concentration, and impacts, quantification of all parameters is not possible at the same time. Field investigation is not possible during flood occurrence, neither temporal variation of all parameters can be captured. To this end, aiming to floor the discussions on the pertinent aspect of flood vulnerability to riparian buildings, we considered inundation depth and flow velocity as random variables and performed finite element analysis using nonlinear static analysis for the dead, live, hydrostatic, and impulsive loadings. Both inundation depth and flow velocity are considered uniformly distributed independent variables. The product of these two random variables is depicted as the IM to create fragility functions. Since interdependencies between inundation depth and flow velocity are rather challenging to be established, we considered these variables as independent random variables and considered the variation encapsulated in one of them does not necessarily affect the other. The variations considered for inundation depth and flow velocity led to estimation of demands for nonlinear static analysis. The estimated demands can be used to construct fragility functions based on the capacities estimated from pushover analysis. Using the demand and capacity responses, we created fragility functions considering momentum flux as the IM, since inundation depth alone would not be representative enough to depict the flooding scenario in steep mountains. The capacity of the building was determined by pushover analysis. The yield and ultimate forces were obtained and three damage states: moderate, extensive, and collapse state capacities were determined from the yield force, average value of yield and ultimate forces, and ultimate force, respectively, per the HAZUS Tsunami Model Technical Guidance (Federal Emergency Management Authority 2017). The demand and capacity ratios were fitted to create lognormal fragility curve for moderate, extensive, and collapse limit states as shown in Fig. 15. The fragility functions shown in Fig. 15 exhibit that the likelihood of moderate damage is quite high even at
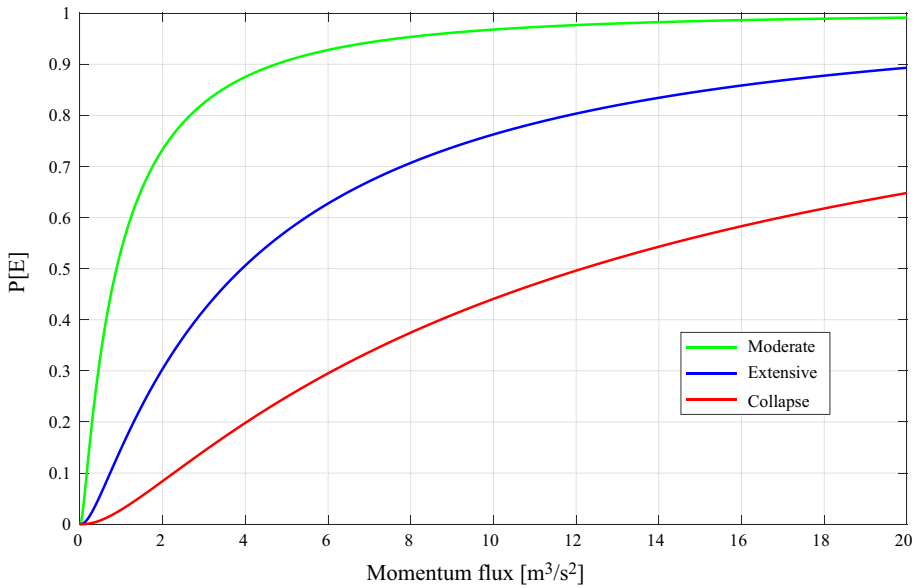
Fig. 15 Analytical flood fragility functions for RC buildings

small momentum fluxes. For example, at 2 m³/s², exceedance probabilities of moderate, extensive, and collapse limit states are, respectively, 74%, 30%, and 18%.

Fragility functions are better explained by momentum flux when considered as IM rather than inundation depth, which is well reflected in terms of exceedance probabilities of all three damage states for various momentum flux scenarios. The fragility models constructed using momentum flux as IM adhere more toward the realistic scenario since velocity undoubtedly plays an instrumental role in structural damage. On the other hand, the analytical fragility models developed using inundation depth solely could suffer from uncertainties arising from fluid–structure interaction, spatial variation of velocity, impulsive actions, and hydrodynamic fluctuations. To this end, analytical fragility models are better explained by momentum flux as IM. However, the fragility functions presented in this research are yet preliminary in nature as we do not consider structural uncertainties and we have not modeled fluid–structure interaction, fluctuation in flow velocity, fluctuation in sediment concentration, impulsive actions due to sediments of various sizes, among others. The aim of presenting the analytical fragility is also to start discussions regarding flood vulnerability of riparian buildings, especially in debris-laden flood regimes, and to identify areas for improvement in the future. Further advancements are fundamentally needed to address the uncertainties and also to define the complexities arising due to localized actions, changes in flow velocity dynamics after impact, and exposure and flood time history.

4 Conclusions

Floods pose great threat to buildings and other infrastructures. Although, in most cases, the geographical extent of damage caused by floods is not as widespread as that from earthquakes, they can devastate riparian communities. High-velocity debris-laden floods

in steep topographies pose an array of challenges to civil engineering structures. Such floods present distinctly different loading and damage mechanisms to riparian constructions than storm surge and tsunami flooding to coastal constructions, but have not been adequately addressed in the literature. We use empirical observations from a recent flood in central Nepal to demonstrate the extent of damage caused by such floods even to engineering reinforced concrete structures. Examples and impacts of different damage mechanisms such as debris settlement, debris impact, flow divergence, etc., are illustrated with observations from the field. Our observations conclude that when the flow is relatively slow, even heavily debris-laden flows are less likely to damage the structural components of an RC building. However, they can result in grave loss of functionality. When the flow velocity is high and debris size is large, structural integrity is often compromised. Apart from this, secondary effects such as toe cutting and foundation erosion become relevant in the case of riparian settlements. A preliminary model for vulnerability, loss of functionality, and fragility of RC buildings affected by the 2021 Melamchi River flood is created by using inundation depth as an intensity measure. This is only a preliminary model because inundation depth alone does not capture the array of effects caused by variability in flow speed and debris size. Analytical fragility functions for typical riparian RC buildings are also created considering various flooding scenarios. The analytical fragility functions developed using momentum flux as IM could be insightful in enriching understanding regarding debris-laden floods in steep topographies. Future research in this area therefore needs to focus on multiple intensity measures to create fragility surfaces or fragility curves conditioned on more than one variable. Our results show that inundation as low as 1.5 m can result in significant damage to RC buildings, and at the same time a large loss in functionality, primarily due to debris accumulation. Although the vulnerability and functionality loss models presented here are based on inundation depth alone, when they are used in conjunction, some uncertainties associated with debris concentration would be accounted for. This is because, high debris concentration might not necessarily lead to structural damage but is likely to result in functionality loss. Being an emerging area of research, the models presented herein are preliminary and should be taken as starting points for potential improvements, both in terms of the volume of empirical evidence and theoretical modeling. Functionality loss, which has a direct consequence on societal resilience, is an evolving process. Although we present a model for it as a snapshot in time a week after the flood, we stress the importance of repeated observations to capture its evolving nature. Such studies can provide valuable insights into repair/restoration campaigns (see, e. g., Rupakhety and Sigbjörnsson (2014)) as well as in formulating disaster mitigation plans, for example, provisions for temporary shelter.

Declarations

Competing interest The authors have no relevant financial or non-financial interests to disclose.

References

Adhikari R, Gautam D, Jha P, Aryal B, Ghalan K, Rupakhety R, Dong Y, Rodrigues H, Motra G (2019) Bridging multi-hazard vulnerability and sustainability: approaches and applications to nepali highway bridges. In Resilient Struct Infrastruct. https://doi.org/10.1007/978-981-13-7446-3_14

Amadio M, Scorzini AR, Carisi F, Essenfelder HA, Domeneghetti A, Mysiak J, Castellarin A (2019) Testing empirical and synthetic flood damage models: the case of Italy. Nat Hazards Earth Syst Sci. https://doi.org/10.5194/nhess-19-661-2019

Bessason B, Rupakhety R, Bjarnason JÖ (2022) Comparison and modelling of building losses in south iceland caused by different size earthquakes. J Build Eng. https://doi.org/10.1016/j.jobe.2021.103806

Ciurean RL, Hussin H, van Westen CJ, Jaboyedoff M, Nicolet P, Chen L, Frigerio S, Glade T (2017) Multi-Scale Debris Flow Vulnerability Assessment and Direct Loss Estimation of Buildings in the Eastern Italian Alps. Nat Hazards. https://doi.org/10.1007/s11069-016-2612-6

Computers and Structures Inc (2013) SAP2000. CSI Inc

del Gaudio C, de Risi MT, Ricci P, Verderame GM (2019) Empirical drift-fragility functions and loss estimation for infills in reinforced concrete frames under seismic loading. Bullet Earthq Eng. https://doi.org/10.1007/s10518-018-0501-y

Federal Emergency Management Authority (2017) Hazus tsunami model technical guidance. United States

Fuchs S, Keiler M, Ortlepp R, Schinke R, Papathoma-Köhle M (2019a) Recent advances in vulnerability assessment for the built environment exposed to torrential hazards: challenges and the way forward. J Hydrol. https://doi.org/10.1016/j.jhydrol.2019.05.067

Fuchs S, Heiser M, Schlögl M, Zischg A, Papathoma-Köhle M, Keiler M (2019b) Short communication: a model to predict flood loss in mountain areas. Environ Model Softw. https://doi.org/10.1016/j.envsoft.2019.03.026

Gautam D (2018) Observational fragility functions for residential stone masonry buildings in Nepal. Bullet Earthq Eng. https://doi.org/10.1007/s10518-018-0372-2

Gautam D, Dong Y (2018) Multi-hazard vulnerability of structures and lifelines due to the 2015 Gorkha earthquake and 2017 central Nepal flash flood. J Build Eng 17:196–201. https://doi.org/10.1016/j.jobe.2018.02.016

Gautam D, Rupakhety R (2021) Empirical seismic vulnerability analysis of infrastructure systems in Nepal. Bull Earthq Eng. https://doi.org/10.1007/s10518-021-01219-5

Gautam D, Fabbrocino G, Santucci de Magistris F (2018) Derive empirical fragility functions for Nepali residential buildings. Eng Struct 171:617–628. https://doi.org/10.1016/j.engstruct.2018.06.018

Gautam D, Rupakhety R, Adhikari R (2019) Empirical fragility functions for Nepali highway bridges affected by the 2015 Gorkha earthquake. Soil Dyn Earthq Eng. https://doi.org/10.1016/j.soildyn.2019.105778

Gautam D, Adhikari R, Jha P, Rupakhety R, Yadav M (2020) Windstorm vulnerability of residential buildings and infrastructures in south-central Nepal. J Wind Eng Indus Aerodyn. https://doi.org/10.1016/j.jweia.2020.104113

Gautam D, Adhikari R, Rupakhety R (2021) Seismic fragility of structural and non-structural elements of Nepali RC buildings. Eng Struct. https://doi.org/10.1016/j.engstruct.2021.111879

Godfrey A, Ciurean RL, van Westen CJ, Kingma NC, Glade T (2015) Assessing vulnerability of buildings to hydro-meteorological hazards using an expert based approach - an application in Nehoiu valley, Romania. Int J Disaster Risk Reduct. https://doi.org/10.1016/j.ijdrr.2015.06.001

Jakob M, Stein D, Ulmi M (2012) Vulnerability of buildings to debris flow impact. Natural Hazards. https://doi.org/10.1007/s11069-011-0007-2

Kang HS, Kim YT (2016) The physical vulnerability of different types of building structure to debris flow events. Nat Hazards. https://doi.org/10.1007/s11069-015-2032-z

Karafagka S, Fotopoulou S, Pitilakis K (2018) Analytical tsunami fragility curves for seaport RC buildings and steel light frame warehouses. Soil Dyn Earthq Eng. https://doi.org/10.1016/j.soildyn.2018.04.037

Komolafe AA, Herath S, Avtar R (2019) Establishment of detailed loss functions for the Urban flood risk assessment in chao phraya river basin, Thailand. Geomatics Nat Hazards Risk. https://doi.org/10.1080/19475705.2018.1539038

Koshimura S, Oie T, Yanagisawa H, Imamura F (2009) Developing fragility functions for tsunami damage estimation using numerical model and post-tsunami data from banda aceh, Indonesia. Coast Eng J. https://doi.org/10.1142/S0578563409002004

Pandey V, Gautam D, Gautam S, Adhikari R, Lamsal P, Talchabhadel R, Bijaya P et al. (2021) Multi-perspective field reconnaissance after the melamchi debris flow of June 15, 2021 in central Nepal. Lalitpur.

Park H, Cox DT, Barbosa AR (2017) Comparison of inundation depth and momentum flux based fragilities for probabilistic tsunami damage assessment and uncertainty analysis. Coast Eng. https://doi.org/10.1016/j.coastaleng.2017.01.008

Petrone C, Rossetto T, Goda K (2017) Fragility assessment of a RC structure under tsunami actions via non-linear static and dynamic analyses. Eng Struct. https://doi.org/10.1016/j.engstruct.2017.01.013

Porter K, Kennedy R, Bachman R (2007) Creating fragility functions for performance-based earthquake engineering. Earthq Spect. https://doi.org/10.1193/12720892

Prieto JA, Journeay M, Acevedo AB, Arbelaez JD, Ulmi M (2018) development of structural debris flow fragility curves (debris flow buildings resistance) using momentum flux rate as a hazard parameter. Eng Geol. https://doi.org/10.1016/j.enggeo.2018.03.014

Reese S, Bradley BA, Bind J, Smart G, Power W, Sturman J (2011) Empirical building fragilities from observed damage in the 2009 south pacific tsunami. Earth Sci Rev. https://doi.org/10.1016/j.earscirev.2011.01.009

Rupakhety R, Sigbjörnsson R (2014) Quantification of loss and gain in performance using survey data: a study of earthquake-induced damage and restoration of residential buildings. Nat Hazards. https://doi.org/10.1007/s11069-014-1279-0

Santo A, N, Santangelo, G Forte, and M de Falco. (2016) Post flash flood survey: the 14th and 15th october 2015 event in the paupisi-solopaca area (Southern Italy). J Maps. https://doi.org/10.1080/17445647.2016.1249034

Shinozuka M, Feng MQ, Lee J, Naganuma T (2002) Statistical analysis of fragility curves. J Eng Mech. https://doi.org/10.1061/(asce)0733-9399(2000)126:12(1224)

Suppasri A, Mas E, Koshimura S, Imai K, Harada K, Imamura F (2012) Developing tsunami fragility curves from the surveyed data of the 2011 great east japan tsunami in sendai and ishinomaki plains. Coast Eng J. https://doi.org/10.1142/S0578563412500088

Thapa S, Shrestha A, Lamichhane S, Adhikari R, Gautam D (2020) Catchment-scale flood hazard mapping and flood vulnerability analysis of residential buildings: the case of khando river in eastern Nepal. J Hydrol: Region Studies. https://doi.org/10.1016/j.ejrh.2020.100704

Valencia N, Gardi A, Gauraz A, Leone F, Guillande R (2011) New tsunami damage functions developed in the framework of SCHEMA project: application to European-mediterranean coasts. Nat Hazards Earth Syst Sci. https://doi.org/10.5194/nhess-11-2835-2011

Authors and Affiliations

Dipendra Gautam[1,2,3] 🔘 · **Rabindra Adhikari**[1,2,4] · **Suraj Gautam**[5] ·
Vishnu Prasad Pandey[2,4] · **Bhesh Raj Thapa**[2,6] · **Suraj Lamichhane**[2,4] ·
Rocky Talchabhadel[2,7] · **Saraswati Thapa**[4,8] · **Sunil Niraula**[9] · **Komal Raj Aryal**[10] ·
Pravin Lamsal[11] · **Subash Bastola**[4] · **Sanjay Kumar Sah**[4] · **Shanti Kala Subedi**[12] ·
Bijaya Puri[2] · **Bidur Kandel**[13] · **Pratap Sapkota**[14] · **Rajesh Rupakhety**[15]

[1]   Department of Civil Engineering, Cosmos College of Management and Technology, Lalitpur, Nepal

[2]   Interdisciplinary Research Institute for Sustainability, IRIS, Kathmandu, Nepal

[3]   Department of Civil Engineering, Institute of Engineering, Thapathali Campus, Kathmandu, Nepal

[4]   Department of Civil Engineering, Institute of Engineering, Pulchowk Campus, Lalitpur, Nepal

[5]   Institute of Himalayan Risk Reduction, Kathmandu, Nepal

[6]   Department of Civil Engineering, Universal Engineering and Science College, Lalitpur, Nepal

[7]   Texas A&M AgriLife Research, Texas A&M University, El Paso, TX, USA

[8]   School of Geosciences, University of Edinburgh, Edinburgh, UK

[9]   Department of Civil Engineering, Himalaya College of Engineering, Lalitpur, Nepal

[10]   Faculty of Resilience, Rabdan Academy, Abu Dhabi, United Arab Emirates

[11]   Geovation Nepal, Kathmandu, Nepal

[12]   Krishnam Smart Engineering Solutions, Kathmandu, Nepal

[13]   Department of Civil Engineering, Nepal Engineering College, Bhaktapur, Nepal

[14]   Nepal Telecom, Kathmandu, Nepal

[15]   Earthquake Engineering Research Center, Faculty of Civil and Environmental Engineering, University of Iceland, Selfoss, Iceland